Inhibition of negative differential resistance in modulation-doped *n*-type $Ga_xIn_{1-x}N_yAs_{1-y}$/GaAs quantum wells

Y. Sun,[1] M. P. Vaughan,[1] A. Agarwal,[1] M. Yilmaz,[2] B. Ulug,[2] A. Ulug,[2] N. Balkan,[1,*] M. Sopanen,[3] O. Reentilä,[3] M. Mattila,[3] C. Fontaine,[4] and A. Arnoult[4]

[1]*Department of Electronic System Engineering, University of Essex, Wivenhoe Park, Colchester CO4 3SQ, United Kingdom*

[2]*Faculty of Arts & Science, Department of Physics, Akdeniz University, Antalya, Turkey*

[3]*Micro and Nanosciences Laboratory, Helsinki University of Technology, P.O. Box 3500, Helsinki 02015, Finland*

[4]*Laboratory for Analysis and Architecture of System, 7 Avenue du Colonel Roche, 31077 Toulouse Cedex 4, France*

(Received 2 October 2006; published 11 May 2007)

We present the results of hot-electron momentum relaxation studies for longitudinal transport in modulation doped $Ga_xIn_{1-x}N_yAs_{1-y}$/GaAs quantum wells. Experimental results show that the high field drift velocity saturates at a value close to 1×10^7 cm/s with no evidence for negative differential resistance or instabilities. Experimental results are compared with a simple theoretical model for transport taking into account the effect of nonequilibrium phonon production. Model calculations indicate that enhanced momentum scattering for electrons with nondrifting hot phonons may be the cause for the reduction in drift velocity.

DOI: 10.1103/PhysRevB.75.205316 PACS number(s): 73.40.−c, 73.50.Fq, 73.21.Fg

I. INTRODUCTION

During the past decade there has been an ever increasing interest in dilute nitrides, particularly in the quaternary material system of GaInNAs/GaAs.[1] This is partly due to the interesting band structure and the revealing novel physical effects associated with the presence of nitrogen, and partly to the evident potential of dilute nitrides for advanced telecommunication device applications.[2–5] In order to analyze and improve the design of functional devices and further predict the ultrafast novel devices based on these materials, a through understanding of electron transport, particularly at high electric fields, is necessary. Hot-electron dynamics for longitudinal transport in degenerate two-dimensional (2D) GaAs and III-N structures are well documented, where the production of nonequilibrium LO phonons (hot phonons) is well known to slow down the hot-electron energy relaxation.[6–10] It is also shown that at high electric fields, the randomization of the hot phonon distribution may take place via the elastic scattering of phonons with, for instance, interface roughness and alloy fluctuations, hence the drift of hot phonons can be neglected. If the momentum relaxation of phonons is faster than their decay time, the change in the electron momentum between the emission and reabsorption of hot phonons can be quite large. Hence, the production of hot phonons with a finite lifetime may also enhance the momentum relaxation rate. The electron drift velocity at high fields is therefore reduced and consequently, the intervalley and real-space transfer negative differential resistances may be quenched.

In dilute nitrides, the almost inevitable presence of nitrogen clusters, impurities, interface imperfections, and dislocations will provide ample sources for phonon momentum scattering. The population of nonequilibrium phonons is therefore expected to be strongly nondrifting, particularly in the region where hot phonon effects are important. Therefore, the reduction in the high-field drift velocity saturation is expected and the negative differential resistance may be inhibited.[7,11] The aim of the work presented here is to give the results of our current experiment on the hot-electron transport in *n*-type modulation-doped $Ga_{1-x}In_xN_yAs_{1-y}$/GaAs quantum wells and to explore whether the observed electron drift velocity at high fields can also be explained by invoking a similar mechanism involving the production of nondrifting hot phonons.

II. EXPERIMENT

The layer structures of the samples used in the investigations are shown in Fig. 1. Two similar structures with varying nitrogen composition in the triple $Ga_{1-x}In_xN_yAs_{1-y}$ quantum wells were grown by molecular-beam epitaxy (sample A) and metal-organic vapor-phase epitaxy (sample B) on semi-insulating GaAs substrate. The mole fraction of nitrogen in the $Ga_{0.7}In_{0.3}N_yAs_{1-y}$ quantum well (QW) is $y=1.5\%$ and $y=1.0\%$ for samples A and B, respectively. Neither of the samples underwent rapid thermal annealing or slow thermal annealing.

The cw photoluminescence (PL) spectra were measured as a function of temperature to establish (a) the presence of the $Ga_{1-x}In_xN_yAs_{1-y}$ quantum wells and (b) their enhanced optical quality compared to undoped material where exciton trapping dominates the optical transitions at low temperatures.[12] Figure 2(a) shows the PL spectra for both samples measured at $T=10$ K. It is clear from the two spectra that the peak wavelength of the QW emission is longer

Material	Thickness (Å)	Doping (cm^{-3})	
GaAs (Cap)	500	Si: $1x10^{18}$	
GaAs (Barrier)	200	Si: $1x10^{18}$	
GaAs (Spacer)	50	UD	
$Ga_{1-x}In_xN_yAs_{1-y}$ QW	70	UD	x 3
GaAs(Spacer)	50	UD	
GaAs(Barrier)	200	Si: $1x10^{18}$	
GaAs (Buffer)	500	UD	
Semi insulating GaAs Substrate			

FIG. 1. The structures of the samples. Sample A: $x=30\%$ and $y=1.5\%$. Sample B: $x=30\%$ and $y=1.0\%$.

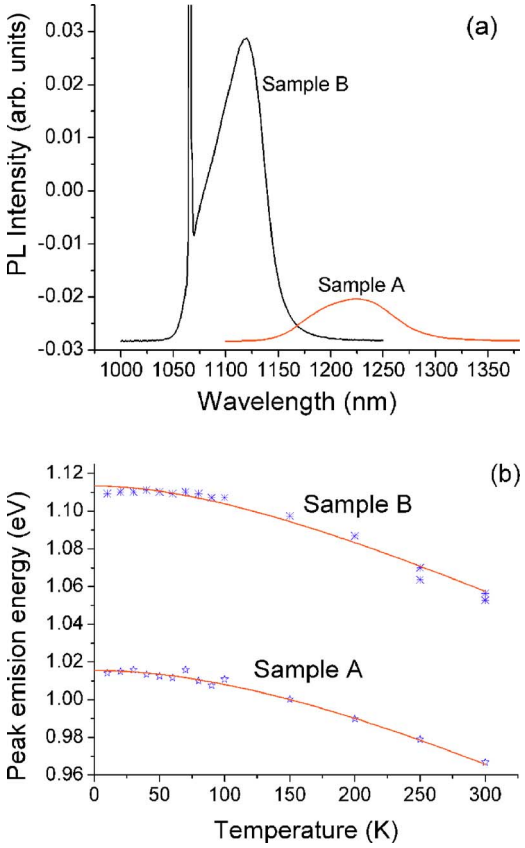

FIG. 2. (Color online) (a) PL spectra of two *n*-type modulation-doped $Ga_{0.7}In_{0.3}N_yAs_{1-y}$/GaAs MQWs with $y=1.5\%$ (sample A) and 1.0% (sample B) measured at 10 K, respectively. The sharp spike in the spectrum for sample B is due to the excitation laser. (b) Temperature dependence of the PL peak energies of sample B (star) and sample A (pentagram). The lines represent the best fit using the Varshni formula (Ref. 15).

with a wider full width at half maximum for sample A with higher nitrogen content but the intensity is about a factor of 10 smaller compared to sample B. These observations are in accordance with the widely studied and reported behavior of dilute nitride systems.[1,12–14] What is most interesting about the PL spectra of the modulation-doped QWs is the lack of the *S*-type behavior that occurs as a result of exciton trapping in these highly disordered systems.[12] The reason for this is the modulation doping and hence the high electron density in the QWs screening efficiently the interband (trapped exciton) transitions. Therefore, the temperature dependence of the PL peak represents better the temperature dependence of the energy gap of the $Ga_{0.7}In_{0.3}N_yAs_{1-y}$ QWs.[13,14] Indeed, the observed behavior can be fitted almost perfectly by an empirical relation between the band gap and temperature, proposed by Potter and Balkan,[12] Polimeni, *et al.*[15] and Varshni,[16] where the size quantization effect on the subband energies is taken into account.

In order to determine the 2D nature of the electrical conductivity and measure the carrier density and Hall mobility, we carried out conventional Hall measurements in both studied samples. Samples are fabricated in the form of Hall bars with channel length of 1.75 mm and width of <0.2 mm.

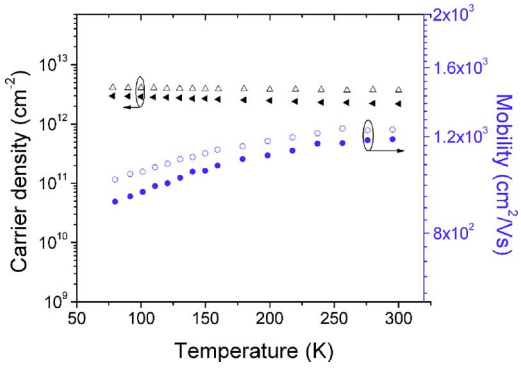

FIG. 3. (Color online) Temperature dependence of sheet carrier density and low-field Hall mobility of sample B (open symbols) and sample A (solid symbols).

Ohmic contacts were formed by alloying Au, Au/Ge, and Ni. Measurements were recorded at lattice temperatures between 77 and 300 K at low enough applied electric fields to avoid any significant carrier heating effects. Indeed, both the Hall mobility and carrier density were independent of applied field within our range of Hall measurements. Figure 3 shows the Hall mobility and sheet carrier density of two samples plotted against the lattice temperature. Electron density is independent of temperature within the experimental accuracy indicating that the conductivity is dominated by the 2D electron transport in the modulation-doped quantum wells. Although both samples are structurally identical and equally modulation doped by Si to 1×10^{18} cm^{-3}, sample A with higher nitrogen content has about a factor of 1.4 lower free electron density. This is indicative of enhanced nitrogen-induced trap density in sample as supported by the reduced intensity of the PL in Fig. 2(a).

The electron mobility is higher than the results by Li *et al.* due to carriers in 2D system that experienced strongly reduced ionized impurity scattering,[17] and slightly increases with the increasing temperature over the range of 77–300 K. Although the high-temperature mobility is likely to be limited by alloy and polar optical-phonon scatterings, both these have monotonically decreasing temperature dependencies. The low-*T* mobility is therefore probably limited by some form of defect scattering, similar to the local impurity type of scattering within the quantum well.[18] The real nature of the dominant scattering mechanism cannot be deduced solely from the Hall measurements; however, local impurities, alloy fluctuations, interface roughness, or any defect associated with localized nitrogen clusters may all give rise to behavior similar to the observed temperature dependence.[18] It is clear that the low-temperature mobility in sample B is about a factor of 1.2 higher than that in sample A. This is due to the screening effect of the higher 2D electron density in sample B and the reduced defect and/or scattering centers in sample B with 1% nitrogen compared to sample A with 1.5% nitrogen.

High speed *I*-*V* measurements were carried out using several simple bars with lengths ranging from 26 to 100 μm. In order to reduce Joule heating, electric-field pulses of 70 ns duration with a duty cycle less than 10^{-5} s were applied along the simple bars. The drift velocity (V_d) as a function of

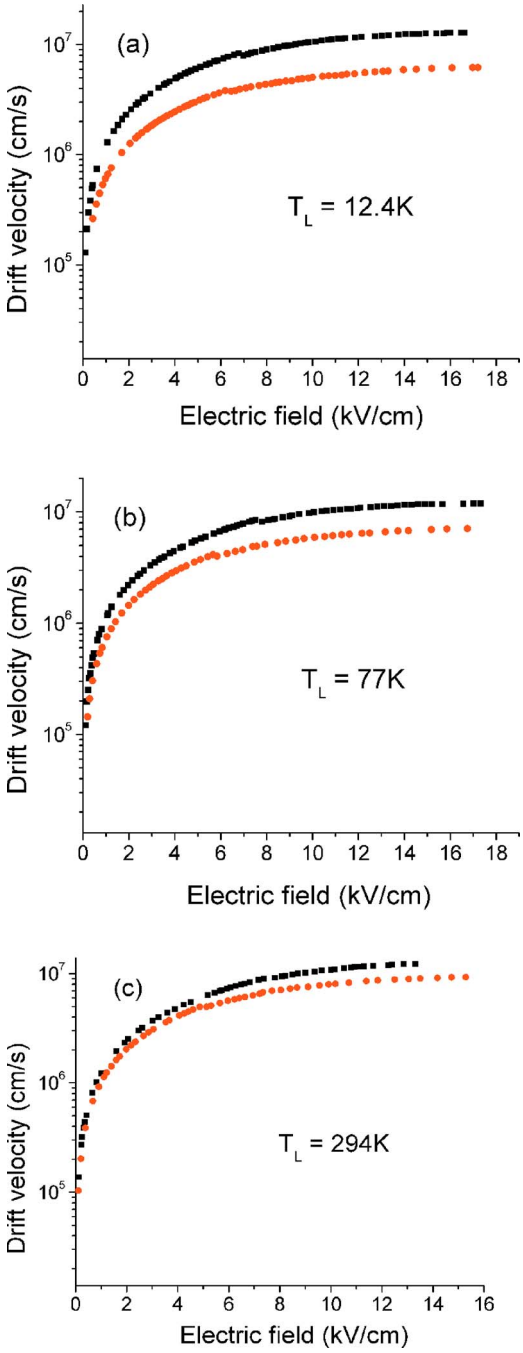

FIG. 4. (Color online) Measured drift velocity versus applied field at T_L=12.4 K, T_L=77 K, and T_L=300 K for samples B (solid squares) and A (solid circles). The inset shows the measured drift velocity as a function of applied field for sample B (solid squares) and sample A (solid circle) on linear scale and the arrows indicate the saturation drift velocities.

applied field was obtained directly from the measured *I-V* characteristics using the electron density measured with the Hall technique. It was assumed, therefore, that the electron concentration remains constant in the measurement range and that the *I-V* characteristics reflect solely the change of electron mobility with electric field.

In Figs. 4(a)–4(c), the measured drift velocity in the two samples investigated is plotted against the applied field at lattice temperatures of 12.4, 77, and 300 K, respectively. The drift velocity first increases linearly with electric field F at low fields (Ohmic region); it then deviates from linearity as expected from increased momentum scattering of hot electrons with LO phonons and finally reaches saturation. Measurement on several simple bars with different channel lengths exhibited the same behavior. The approximate saturation drift velocities (V_{ds}) obtained in the two structures are listed, together with the corresponding electric fields at different lattice temperatures in Table I.

The results in Figs. 4(a)–4(c) coupled with those summarized in Table I clearly indicate that the saturation drift velocity and the corresponding electric fields strongly depend on nitrogen concentration and carrier density. The drift velocities of sample B reach saturation at lower electric fields than that of sample A at all measured lattice temperatures due to higher carrier density; hence, the enhanced hot phonon effects, as described below. The negative differential conductivity via real-space transfer or intervalley transfer is suppressed and no negative differential velocity effect. This observation should be distinguished from the results by Patane *et al.* which are explained by using an eloquent model for NDR associated with negative effective mass arising from the high nonparabolic band structure in dilute nitrides.[19–21] It should also be noted that those structures were either undoped or lightly doped bulk material where hot phonon effects would be negligible.

III. THEORY AND THE DISCUSSION OF RESULTS

The model used in the calculations is based on the energy and momentum balance methods, in which the energy and momentum rates are averaged over a drifted Maxwellian distribution.[22] Assuming the average displacement of the electron distribution is in the direction of the applied field F, the energy and momentum balance equations are

$$\left\langle \frac{dE}{dt} \right\rangle = eV_dF = R_E = f(T_e),$$

$$\left\langle \frac{d\hbar k}{dt} \right\rangle = eF = R_p, \tag{1}$$

where V_d, E, and $\hbar k$ are the drift velocity electron energy and momentum, respectively, and e is the electronic charge. For simplicity, we restrict attention to electrons in a single parabolic band interacting solely with polar-optical-phonon scattering for energy relaxation (see below for discussion of our assumption of parabolicity). For momentum relaxation, a further elastic scattering rate is incorporated to correct the low-field mobility. It is found that for a parabolic band, after averaging over the drifted electron distribution, the momentum relaxation rate for a given process i is a function of electron temperature (T_e),

$$R_p = \sum_i R_p^i = V_d \sum_i h_i(T_e) = V_d h(T_e). \tag{2}$$

For simplicity, we assume that electrons are confined to the lowest subband in a deep square quantum well and the inter-

TABLE I. Saturation drift velocities in the two samples at different lattice temperatures.

	Temperature					
	12.4 K		77 K		294 K	
Sample	V_{ds} (cm/s)	F (kV/cm)	V_{ds} (cm/s)	F (kV/cm)	V_{ds} (cm/s)	F (kV/cm)
B	1.28×10^7	14.9	1.17×10^7	14.6	1.22×10^7	12.4
A	0.62×10^7	16.9	0.71×10^7	16.7	0.96×10^7	15.3

action with phonons is confined to the same quantum well. The energy relaxation rate for polar-optical scattering then can be written as[8]

$$eFV_d = f_{PO}(T_e) = \frac{\hbar\omega}{\tau_0}\left(\frac{E_L}{\hbar\omega}\right)^{1/2}\left\{[n(\omega)+1]\exp\left(-\frac{\hbar\omega}{k_BT_e}\right)-n(\omega)\right\}, \tag{3}$$

where $\hbar\omega$ is the LO phonon energy, $n(\omega)$ is the phonon occupancy (determined by electron temperature), $E_L = \hbar^2\pi^2/2m^*L^2$ is the energy shift of the lowest subband in an infinitely deep well of width L, and k_B is Boltzmann's constant. τ_0 is a characteristic time constant for the polar interaction given by

$$\tau_0 = \frac{e^2\omega}{2\pi\hbar}\left(\frac{m^*}{2\hbar\omega}\right)^{1/2}\left(\frac{1}{\varepsilon_\infty}-\frac{1}{\varepsilon_s}\right), \tag{4}$$

where ε_∞ and ε_s are the high-frequency and static permittivities, respectively, and m^* is the effective electron mass. The effect of a population of nondrifted hot phonons can be incorporated by substituting for $n(\omega)$ using the expression for hot phonon occupation derived by Ridley[8]

$$n(\omega) = \frac{n_0(\omega)+(\tau_p/2\tau_0q_0L)(\pi k_BT_e/\hbar\omega)^{1/2}(n/N_c)\exp(-\hbar\omega/k_BT_e)}{1+(\tau_p/2\tau_0q_0L)(\pi k_BT_e/\hbar\omega)^{1/2}(n/N_c)[1-\exp(-\hbar\omega/k_BT_e)]}, \tag{5}$$

where τ_p is the model phonon lifetime, n is the bulk electron density, $q_0=(2m^*\hbar\omega)^{1/2}/\hbar$ is the phase-matched phonon wave vector, and $N_c=m^*k_BT_e/\pi\hbar^2L$ is an effective density of states. The equilibrium phonon occupation number $n_0(\omega)$ is given, as usual, by the Bose-Einstein factor $n_0(\omega) = 1/[\exp(\hbar\omega/k_BT_0)-1]$. Note that it is the electron density that essentially determines the hot phonon effects. Substituting for $n(\omega)$ from Eq. (5) into Eq. (3) gives

$$eFV_d = f_{PO}(T_e) = \frac{\hbar\omega}{\tau^*}\left(\frac{E_L}{\hbar\omega}\right)^{1/2}\left\{[n_0(\omega)+1]\exp\left(-\frac{\hbar\omega}{k_BT_e}\right)-n_0(\omega)\right\}, \tag{6}$$

where the effective energy relaxation time τ^* which takes into account all the hot phonon effects is given by

$$\tau^* = \tau_0 + \left(\frac{\tau_p n}{2q_0LN_c}\right)\left(\frac{\pi k_BT_e}{\hbar\omega}\right)^{1/2}\left[1-\exp\left(-\frac{\hbar\omega}{k_BT_e}\right)\right]. \tag{7}$$

The momentum relaxation rate via the interaction with optical phonons can be found using[8]

$$h_{PO}(T_e) = \frac{m^*(\hbar\omega E_L)^{1/2}}{\tau_0k_BT_e}[n(\omega)+1]\exp(-\hbar\omega/k_BT_e). \tag{8}$$

Substituting for $n(\omega)$ from Eq. (5) gives

$$h_{PO}(T_e) = \frac{m^*(\hbar\omega E_L)^{1/2}}{\tau^*k_BT_e}\left[n_0(\omega)+1+(\tau_p/2q_0\tau_0L)\times(\pi k_BT_e/\hbar\omega)^{1/2}\frac{n}{N_c}\right]\exp(-\hbar\omega/k_BT_e). \tag{9}$$

In addition to the electron-LO phonon scattering, a further elastic scattering rate with an arbitrary temperature dependence can be included by defining $h_e(T_e)=h_e(T_0)(T_e/T_0)^r$, where T_0 is the equilibrium lattice temperature and r can be determined from the best fit to the experimental data. We then have $h(T_e)=h_{PO}(T_e)+h_e(T_e)$. The value of $h_e(T_0)$ can be determined in accordance with the low-field mobility u_0 by

$$h_e(T_0) = \left[\frac{e}{u_0}-h_{PO}(T_0)\right], \tag{10}$$

where $h_{PO}(T_0)$ can be obtained from Eq. (9) in the limit $T_e\to T_0$,

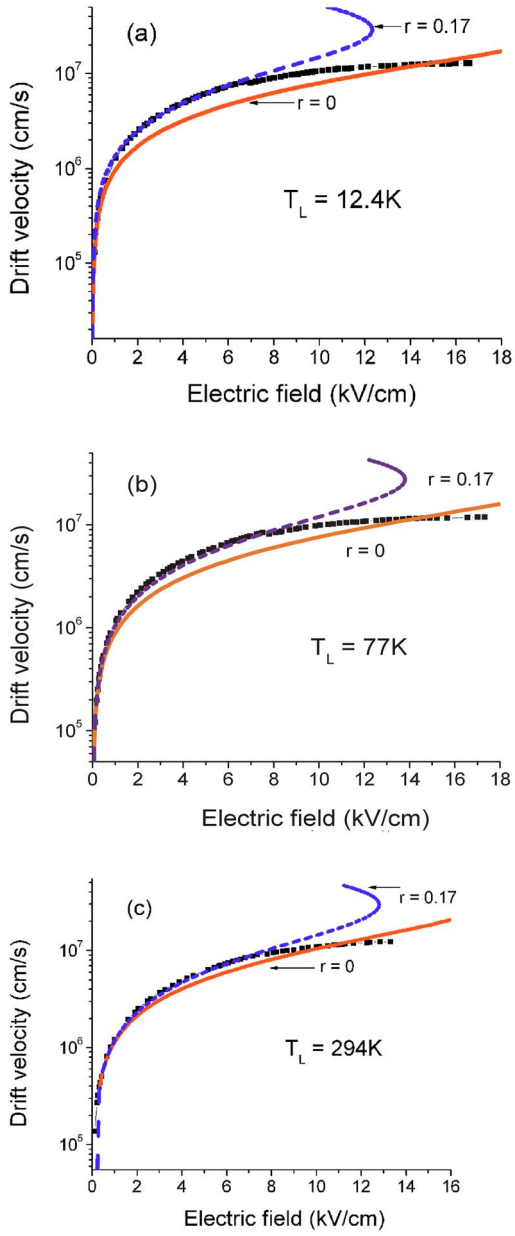

FIG. 5. (Color online) Drift velocity versus applied electric field at lattice temperatures of 12.4, 77, and 294 K for sample B. The solid and broken curves show the calculated drift velocity with $r=0.17$ (broken line) and $r=0$ (solid line), respectively. The solid squares represent the experimental data.

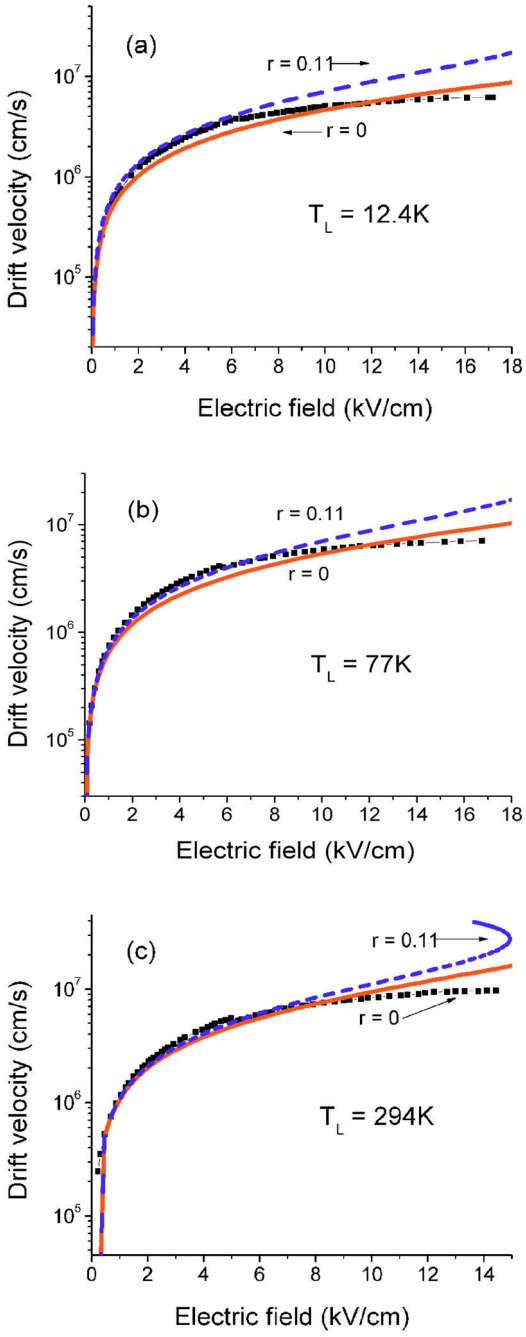

FIG. 6. (Color online) Drift velocity versus applied electric field at lattice temperatures of 12.4, 77, and 294 K for sample A. The solid and broken curves show the calculated drift velocity with $r=0.11$ (broken line) and $r=0$ (solid line), respectively. The solid squares represent the experimental data.

$$h_{PO}(T_0) = \frac{m^*(\hbar\omega E_L)^{1/2}}{\tau_0 k_B T_0} n_0(\omega). \tag{11}$$

The drift velocity can then be found as a function of electron temperature,

$$V_d(T_e) = \frac{eF(T_e)}{h_{PO}(T_e) + \left(\frac{e}{u_0} - h_{PO}(T_0)\right)\left(\frac{T_e}{T_0}\right)^r}. \tag{12}$$

Combining Eqs. (6) and (12) gives an expression relating electron temperature to electric fields; hence, drift velocity versus electric fields curves can be deduced. The model is applied using $\tau_P=7$ ps and quantum-well width $L=7$ nm. [8,23] The phonon energy and dielectric constant are taken to be linear interpolations of the GaAs and InAs values. The effective masses of $m^*=0.0599m_0$ and $0.069m_0$ used for samples B and A, respectively, are calculated from the band-anticrossing model[24] using parameters from Fahy and O'Reilly[25] together with the effective mass for InGaAs inter-

polated using bowing parameters taken from the work of Vurgaftman *et al.*[26]

In Figs. 5(a)–5(c) and 6(a)–6(c), we show the calculated electron drift velocity versus electric field at T_L=12.4, 77, and 294 K for samples B and A, respectively. Also shown in the figures are the experimental results, represented by solid squares. It is clear from the figures that at low fields (low electron temperatures), the experimental data agree very well with the calculated drift velocity curves with r=0.17 for sample B and r=0.11 for sample A, respectively. At high electric fields, as the electron temperature rises, the experimental drift velocities for both samples are suppressed and move closer to the calculated curves with r=0. The highest attainable drift velocity of around $v_{ds}=1.17\times10^7$ cm s^{-1} for sample B is smaller than the peak velocities predicted by Patane *et al.*[21] The model without hot phonons (we simply put τ_P=0 in our calculation) only agrees well with experimental data at low lattice temperature (12.4 K) and predicts a higher drift velocity than the measured values at higher lattice temperatures of 77 and 294 K. However, a hot-electron analysis without the constant momentum relaxation rate (r=0) predicts a runaway at high field with the drift velocity turning up abruptly. This is a typical feature of polar-optical scattering in a parabolic band and may be suppressed with the inclusion of the band nonparabolicity and/or additional energy relaxing processes such as acoustic-phonon scattering. These results coupled with Figs. 5(a)–5(c) and 6(a)–6(c) suggest strongly that some elastic scattering and nonequilibrium population of hot phonons (LO phonons) causes the reduction in the drift velocity.

The model used in this work is based on the assumption of a single parabolic band and that the electronic states are extended. Our primary motivation is not a realistic modeling of hot-electron behavior [for which we should incorporate the nonparabolicity as demonstrated in several works (see, for example, Lindsay and O'Reilly[27])] but to indicate the effect of a population of hot phonons on the drift velocity as stated in the Abstract and Introduction. The effect of the nonparabolicity on the transport properties should become most significant as the average electron energy $\langle E\rangle$ approaches the energy of a localized nitrogen state. The isolated nitrogen state lies about 250 meV above the band edge in GaAs, which translates to about 640 meV above the GaInNAs band edge for the nitrogen concentration of the samples. Taking $\langle E\rangle=3k_BT_e/2$, this gives a hot-electron temperature of about 7000 K, which, in our calculations, corresponds to a field of about 10.5 kV cm^{-1}. It is around this magnitude of field that our parabolic model would begin to fail even for conventional semiconductors due to the hot-electron temperature dependence of the polar-optical (PO)-phonon relaxation rates, which lead to the thermal runaway effects previously reported.[1] Hence, we only attempt to fit our results at lower fields than this where the modified band structure is simply modeled by incorporating the increased effective mass.

Ideally, a comprehensive model of high-field transport should address both the band-structure and the hot-electron temperature dependence of the energy and momentum relaxation times as well as issues such as hot phonons. The simple modeling that we do here can be viewed as a step toward that goal, in advance of more sophisticated models which are underway and will be published in the near future.

IV. SUMMARY

In conclusion, we have studied the energy and momentum relaxations in $Ga_xIn_{1-x}N_yAs_{1-y}$/GaAs quantum-well structures. The results are compared with a theory based on the nondrifting (hot) phonons production. It has been shown that the drift velocity is dependent on the nitrogen concentration and is suppressed at high electric field in both investigated samples. It is argued that this reduction in drift velocity is caused by some elastic scattering and creation of hot phonons due to the existence of necessary sources for phonon momentum relaxation. Consequently, the negative differential conductivity caused by real transfer or intervalley transfer is inhibited. The agreement between the experimental data and the theory is very good. It should be emphasized that the carrier concentration is the principal parameter dictating the hot phonon effect. This increases the suppression of the drift velocity and vice versa. At present, only optical-phonon scattering (which has no adjustable parameters) and an elastic scattering mechanism fitted to the measured low-field mobility are incorporated. A more sophisticated model should include other mobility-limiting processes, most particularly scattering from nitrogen centers. This work will be forthcoming in the near future.

ACKNOWLEDGMENT

We are grateful to B. K. Ridley for fruitful discussions.

*Author to whom correspondence should be addressed. Electronic address: balkan@essex.ac.uk

[1] As review see, J. Phys.: Condens. Matter **16**, 31 (2004), special issue on dilute nitrides.
[2] B. Borchert, A. Y. Egorov, S. Illek, M. Komainda, and H. Riechert, Electron. Lett. **35**, 2204 (1999).
[3] E. Tournie, M.-A. Pinault, M. Laugt, J.-M. Chauveau, A. Trampert, and K. H. Ploog, Appl. Phys. Lett. **82**, 1845 (2003).
[4] A. Wanger, C. Ellmers, F. Hohnsdorf, J. Koch, C. Agert, S. Leu, M. Holfmann, W. Stolz, and W. W. Ruhle, Appl. Phys. Lett. **76**, 271 (2000).
[5] J. S. Harris, Semicond. Sci. Technol. **17**, 880 (2002).
[6] R. Gupta, N. Balkan, and B. K. Ridley, Semicond. Sci. Technol. **7**, 274 (1992).
[7] N. Balkan, R. Gupta, M. E. Daniels, B. K. Ridley, and M. Emeny, Semicond. Sci. Technol. **5**, 986 (1990).
[8] B. K. Ridley, Semicond. Sci. Technol. **4**, 1142 (1989).
[9] R. Gupta and B. K. Ridley, Semicond. Sci. Technol. **9**, 753

(1994).
[10] B. K. Ridley, W. J. Schaff, and L. F. Eastman, J. Appl. Phys. **96**, 1499 (2004).
[11] S. Gokden, N. Balkan, and B. K. Ridley, Semicond. Sci. Technol. **18**, 206 (2003).
[12] R. J. Potter and N. Balkan, J. Phys.: Condens. Matter **16**, 3387 (2004).
[13] H. Haratizadeh, P. P. Paskov, G. Pozina, P. O. Holtz, B. Monemar, S. Kamiyama, M. Iwaya, H. Amano, and I. Akasaki, Appl. Phys. Lett. **80**, 1373 (2002).
[14] A. B. Henriques, Phys. Rev. B **44**, 3340 (1991).
[15] A. Polimeni, M. Capizzi, M. Geddo, M. Fischer, M. Reinhardt, and A. Forchel, Appl. Phys. Lett. **77**, 2870 (2000).
[16] Y. P. Varshni, Physica (Utrecht) **34**, 149 (1967).
[17] W. Li, M. Pessa, J. Toivonen, and Harri Lipsanen, Phys. Rev. B **64**, 113308 (2001).
[18] D. Zanato, S. Gokden, N. Balkan, B. K. Ridley, and W. Schaff, Semicond. Sci. Technol. **19**, 427 (2004).
[19] K. Hess, J. Phys. Colloq. **42**, C7-3 (1981).
[20] B. K. Ridley and T. B. Watkins, Proc. Phys. Soc. London **78**, 293 (1961).
[21] A. Patane, A. Ignatov, D. Fowler, O. Makarovsky, L. Eaves, L. Geelhaar, and H. Riechert, Phys. Rev. B **72**, 033312 (2005).
[22] B. K. Ridley, *Quantum Process in Semiconductors*, 4th ed. (Clarendon, Oxford, 1999).
[23] F. Vallee and F. Bogani, Phys. Rev. B **43**, 12049 (1991).
[24] W. Shan, W. Walukiewicz, J. W. Ager III, E. E. Haller, J. F. Geisz, D. J. Friedman, J. M. Olson, and S. R. Kurtz, Phys. Rev. Lett. **82**, 1221 (1999).
[25] S. Fahy and E. P. O'Reilly, Appl. Phys. Lett. **83**, 3731 (2003).
[26] I. Vurgaftman, J. R. Meyer, and L. R. Ram-Mohan, J. Appl. Phys. **89**, 5815 (2001).
[27] A. Lindsay and E. P. O'Reilly, Phys. Rev. Lett. **93**, 196402 (2004).